Available online at www.sciencedirect.com
ScienceDirect
Journal of the European Ceramic Society 31 (2011) 2137–2143
www.elsevier.com/locate/jeurceramsoc

Mechanical and electrical properties of carbon nanofibers reinforced aluminum nitride composites prepared by plasma activated sintering

Zhongqi Shi *, Shugang Chen, Jiping Wang, Guanjun Qiao, Zhihao Jin

State Key Laboratory for Mechanical Behavior of Materials, School of Materials Science and Engineering, Xi'an Jiaotong University, Xi'an 710049, PR China

Received 14 March 2011; received in revised form 3 May 2011; accepted 15 May 2011
Available online 8 June 2011

Abstract

High density carbon nanofibers (CNFs) reinforced aluminum nitride (AlN) composites were successfully fabricated by plasma activated sintering (PAS) method. The effects of CNFs on the microstructure, mechanical and electrical properties of the AlN composites were investigated. The experimental results showed that the grain growth of AlN was significantly inhibited by the CNFs. With 2 wt.% CNFs added into the composites, the fracture toughness and flexural strength were increased, respectively to 5.03 MPa $m^{1/2}$ and 354 MPa, which were 20.9% and 13.4% higher than those of monolithic AlN. The main toughening mechanisms were CNFs pullout and bridging, and the main reason for the improvements in strength should be the fine-grain-size effect caused by the CNFs. The DC conductivity of the composites was effectively enhanced through the addition of CNFs, and showed a typical percolation behavior with a very low percolation threshold at the CNFs content of about 0.93 wt.% (1.51 vol.%).

Keywords: Carbon nanofibers; B. Composites; C. Mechanical properties; C. Electrical properties; A. Sintering

1. Introduction

Aluminum nitride (AlN), as an important III–V group wide-band-gap semiconductor, has aroused great interest due to its high thermal conductivity, high electrical resistivity, low dielectric constant and low thermal expansion coefficient.[1] However, the applications of AlN ceramic have been restricted due to its inherent brittleness and relative low strength compared with other structural ceramics such as silicon nitride, zirconia, etc.[2] Thus, the mechanical properties (especially fracture toughness and flexural strength) of AlN need to be improved to an acceptable level so as to increase its reliability in service. In addition, for AlN to be used as a functional material for some special applications such as wave-absorbing material, plasma etching electrode, EDM-machinable ceramic substrates and electrical feedthrough, a higher electrical conductivity is required.[3–5]

Ever since their discovery, carbon nanofilaments such as single-wall carbon nanotubes (SWCNTs), multi-wall carbon nanotubes (MWCNTs) and carbon nanofibers (CNFs) have been considered as the most ideal reinforcing or functionalizing elements to improve the mechanical, thermal and electrical properties of ceramic-matrix composites due to their extremely high aspect ratios, low density, high tensile strength, and high thermal and electrical conductivity.[6–8] Therefore, it is expected that the tailoring of carbon nanofilaments into AlN matrix might result in a set of desirable mechanical and electrical properties in AlN for wider application. However, to the best of our knowledge, there has not yet been a report on the fabrication and properties of AlN-carbon nanofilaments system. Among the carbon nanofilaments, CNFs have generated considerable interest in the composite application fields due to their many potential advantages such as low price and good dispersibility compared with SWCNTs and MWCNTs.[9–11] However, most studies to date have confirmed that CNTs can enhance the mechanical and functional properties of ceramic matrix,[12–19] with only limited work having been done on CNFs reinforced ceramic composites. Therefore, it is imperative to explore whether the incorporation of CNFs into AlN matrix could improve the mechanical properties and electrical properties of the AlN composites.

It has been reported that the plasma activated sintering (PAS), also known as spark plasma sintering (SPS), is an efficient method to achieve high density CNTs/ceramic nanocomposites at relatively lower temperature with shorter

* Corresponding author. Tel.: +86 29 8266 5221; fax: +86 29 8266 3453.
E-mail addresses: szqxjtu@gmail.com, zhongqishi@mail.xjtu.edu.cn (Z. Shi).

0955-2219/$ – see front matter © 2011 Elsevier Ltd. All rights reserved.
doi:10.1016/j.jeurceramsoc.2011.05.011

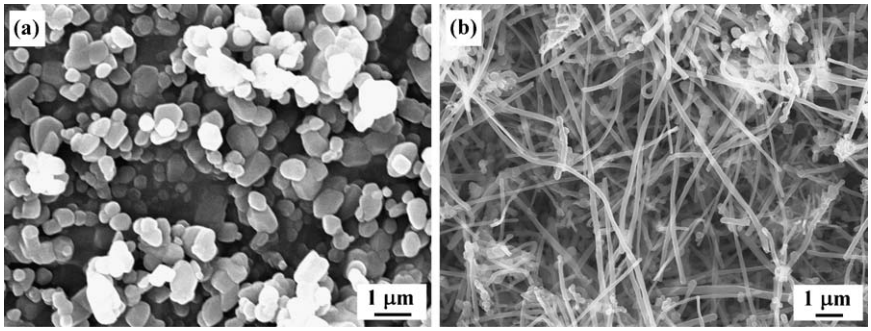

Fig. 1. Morphologies of starting materials: (a) AlN powder and (b) CNFs.

soaking time.[13–15,20,21] Therefore, in this article, PAS method was employed to fabricate CNFs/AlN nanocomposites. The effects of CNFs on the microstructure, mechanical and electrical properties of AlN were carefully investigated.

2. Experimental procedure

High purity AlN powder (type H, >99.9% purity, ~0.5 μm, Tokuyama K.K., Tokyo, Japan) and CNFs ("VGCF–H", ~99% purity, ~150 nm in diameter and 4–5 μm in length, Showa Denko K.K., Tokyo, Japan) were used as the starting powders. The morphologies of AlN powder and CNFs are shown in Fig. 1(a) and (b), respectively. The amount of CNFs ranged from 0 to 7 wt.%. In order to enhance the sinterability, 2 wt.% of CaF_2 (>98.5% purity, ~2 μm, Shanghai Chemistry, Shanghai, China) and 1 wt.% of Y_2O_3 (99.8% purity, <1 μm, Shanghai Yuelong, Non-ferrous Metal Co. Ltd., Shanghai, China) were added as sintering aids. According to the designed composition, CNFs were weighed and dispersed in ethanol, using an ultrasonic bath (power: 250 W) for 30 min. AlN powder and sintering aids were also weighed and dispersed by the same method. Finally, the CNFs suspension was mixed with the AlN powder and the sintering aid slurry, and dispersed for 30 min by ultrasonic bath. The mixed slurry was milled for 12 h using agate balls as milling media, and then dried at 70 °C for 8 h and further sieved to 100 mesh.

The powders were loaded into a graphite die with an inner diameter of 30 mm, and then sintered by PAS (Ed-PASIII, Elenix Ltd., Japan) at 1650 °C (heating speed: 120 °C/min) for 5 min under an uniaxial pressure of 30 MPa in a vacuum (<10^{-2} Pa). A uniaxial pressure of 30 MPa was applied to the powders and kept constant before the as-sintered samples were taken out. The temperature was measured using an optical pyrometer focused on a little hole at the surface of the die. After sintering, the cooling rate was set as 100 °C/min. The as-sintered compacts were cut, ground and polished for the following measurements.

The bulk density of the specimens was measured by the Archimedes immersion technique with deionized water, and the relative density was calculated by the rule of mixtures. The flexural strength was determined by a three-point bending test (sample size 3 mm × 4 mm × 20 mm, span 16 mm, crosshead speed 0.5 mm min^{-1}). The elastic modules was calculated simultaneously using the linear portion of the load–displacement curve. The fracture toughness was determined by the single-edge notched beam (SENB) method (sample size 2 mm × 4 mm × 20 mm, span 16 mm, gap width ≤0.2 mm, gap depth 0.5 ± 0.1 mm). The hardness was determined by means of Vickers indentation method with a load of 49 N for 30 s. At least five specimens were used for each test.

Phase compositions of the as-sintered CNFs/AlN composites were characterized by X-ray diffraction (XRD, X-Pert Pro, Netherlands). Fracture surfaces and the crack propagation paths (produced by Vickers indenter) were observed by field-emission scanning electron microscopy (FE-SEM, JSM-6700F, JEOL, Japan). The electrical conductivity measurements of the composites were performed at room temperature by a DC four-probe technique (Keithley 2400, US).

3. Results and discussion

3.1. Sintering behavior

Fig. 2 shows the *Z*-axis displacement of the CNFs/AlN composites during PAS process as a function of time. The monitoring temperature is also given. The displacement curves show a similar tendency of all the as-sintered samples. The displacement slightly increased at the initial stage owing to the thermal expan-

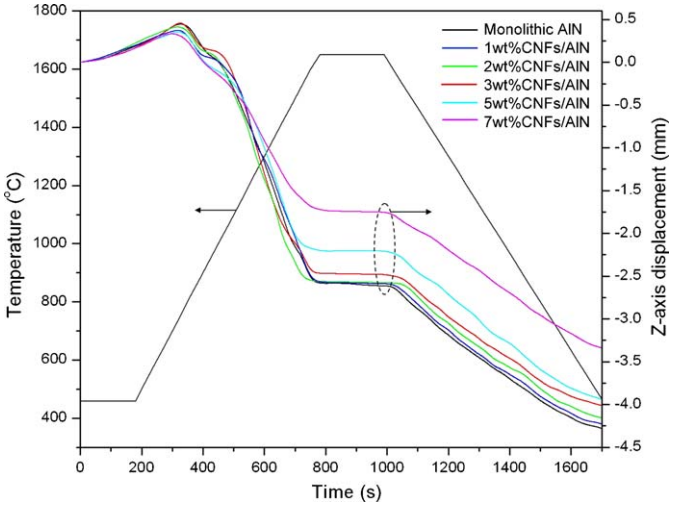

Fig. 2. *Z*-axis displacement curves of different CNFs/AlN composites during PAS process as a function of time.

Table 1
Bulk density and relative density of different CNFs/AlN composites.

Material	Bulk density (g/cm^3)	Relative density (%)
Monolithic AlN	3.26	99.7
1 wt.% CNF/AlN	3.24	99.5
2 wt.% CNF/AlN	3.19	98.6
3 wt.% CNF/AlN	3.14	97.6
5 wt.% CNF/AlN	3.13	98.3
7 wt.% CNF/AlN	2.96	94.2

sion of the samples and the absence of any densification at low temperature, and decreased afterwards when the effect of densification overcame those of thermal expansion. The slight shrinkage in the range of 800–1000 °C might be caused by the rearrangement of the particles under the pressure. With the increase of temperature, liquid phases were formed and wet the nitride particles. A large amount of particles were quickly rearranged by grain boundary sliding under the simultaneous actions of capillary forces and the applied pressure, resulting in a rapid shrinkage. This pronounced shrinkage occurred in the temperature range of 1000–1650 °C and ended at 1650 °C. Thus, the samples were sintered at 1650 °C. Then, a moderate shrinkage was observed for all the samples during the cooling process, which should be associated with the thermal shrinkage of both the samples and the graphite plungers. Fig. 2 also shows that the shrinkages of the samples during sintering were at the same level when the CNFs content dropped below 3 wt.%, while they were gradually restricted when the content was increased to over 5 wt.%.

Table 1 shows the bulk density and relative density of the as-sintered samples. It was noticed that even if the addition of CNFs was up to 5 wt.%, the relative density could still attain 98.3%, indicating that CNFs content below 5 wt.% had no remarkable deleterious effect on the densification process. However, with the CNFs content increased to 7 wt.%, the relative density dropped considerably to 94.2%. The decrease in density should be caused by the high CNFs content which strongly restricted the rearrangement of AlN particles during the sintering process. The results are in accord with the tendency of *Z*-axis displacement curves in Fig. 2.

Fig. 3 shows the XRD patterns of the as-sintered samples. The samples were almost pure AlN phase together with a trace of $CaYAlO_4$ and $Y_4Al_2O_9$ liquid phases formed during the sintering process. The liquid phases strongly promoted the densification of the CNFs/AlN composites, similar to the report of sintering high density AlN ceramics at low temperature with CaF_2 and Y_2O_3 as additives.[22] CNFs could be detected by XRD measurement when its content was over 2 wt.%, which indicated the preservation of CNFs in the composites after PAS. CNFs were not observed when their content was below 2 wt.% in the composites, which might be due to the limitations of the measurement technique.

Fig. 4 shows the fracture surface of the CNFs/AlN composites. The fracture mode of all the composites was predominantly intergranular. CNFs appeared to be distributed homogeneously in the AlN matrix. However, some clusters (marked by arrows in Fig. 4(d)–(f)) could be observed in the composites containing CNFs more than 3 wt.%, and big clusters presented in the composites with 7 wt.% CNFs (see the insert of Fig. 4(f)), which could lead to the lower relative density of the composites. It was, therefore, difficult to induce a well dispersion of CNFs in AlN matrix for the case of the CNFs content more than 3 wt.% by using ultrasonic and ball milling methods. In addition, it was also observed that the AlN grain size decreased with the increase of CNFs content, from about 4 μm for monolithic AlN (Fig. 4(a)) to 2–3 μm for 2 wt.% CNFs/AlN (Fig. 4(c)) and about 1 μm for 7 wt.% CNFs/AlN (Fig. 4(f)). This suggested that the AlN grain growth was significantly inhibited by CNFs during the sintering processing.

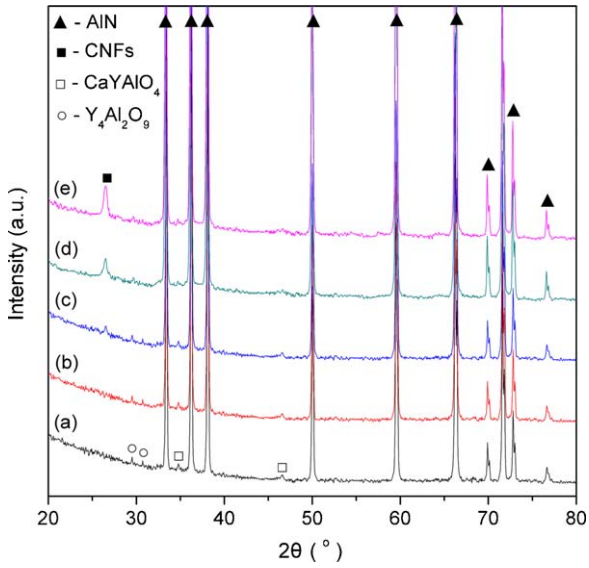

Fig. 3. X-ray diffraction patterns of as-sintered samples: (a) monolithic AlN, (b) 2 wt.% CNFs/AlN, (c) 3 wt.% CNFs/AlN, (d) 5 wt.% CNFs/AlN, (e) 7 wt.% CNFs/AlN.

3.2. Mechanical properties

Fig. 5 shows the fracture toughness, flexural strength, hardness and elastic modulus of the CNFs/AlN composites as a function of CNFs content. The fracture toughness of the composites increased by 20.9% gradually from 4.16 MPa m$^{1/2}$ for monolithic AlN to 5.03 MPa m$^{1/2}$ for 2 wt.% CNFs/AlN composites, indicating the good toughening effect of the CNFs. The toughening mechanisms were clearly explained from the SEM micrographs of the fracture surfaces and the indentation crack propagation paths for the composites. As shown in Fig. 6(a), the CNFs are homogeneously dispersed within the AlN matrix and almost distribute at the grain boundary of 2 wt.% CNFs/AlN composites. There are a large number of residual holes left by the pulling out of the CNFs (indicated by arrows in Fig. 6(a)), indicating the presence of an ideal CNFs–AlN interfacial structure suitable for crack bridging and pullout. Fig. 6(b) shows a typical SEM micrograph of the crack propagation path of 2 wt.% CNF/AlN composites produced by Vickers indentation. The existence of CNFs pullout and bridging in the crack propagation path strongly indicated the crack bridging effect of the

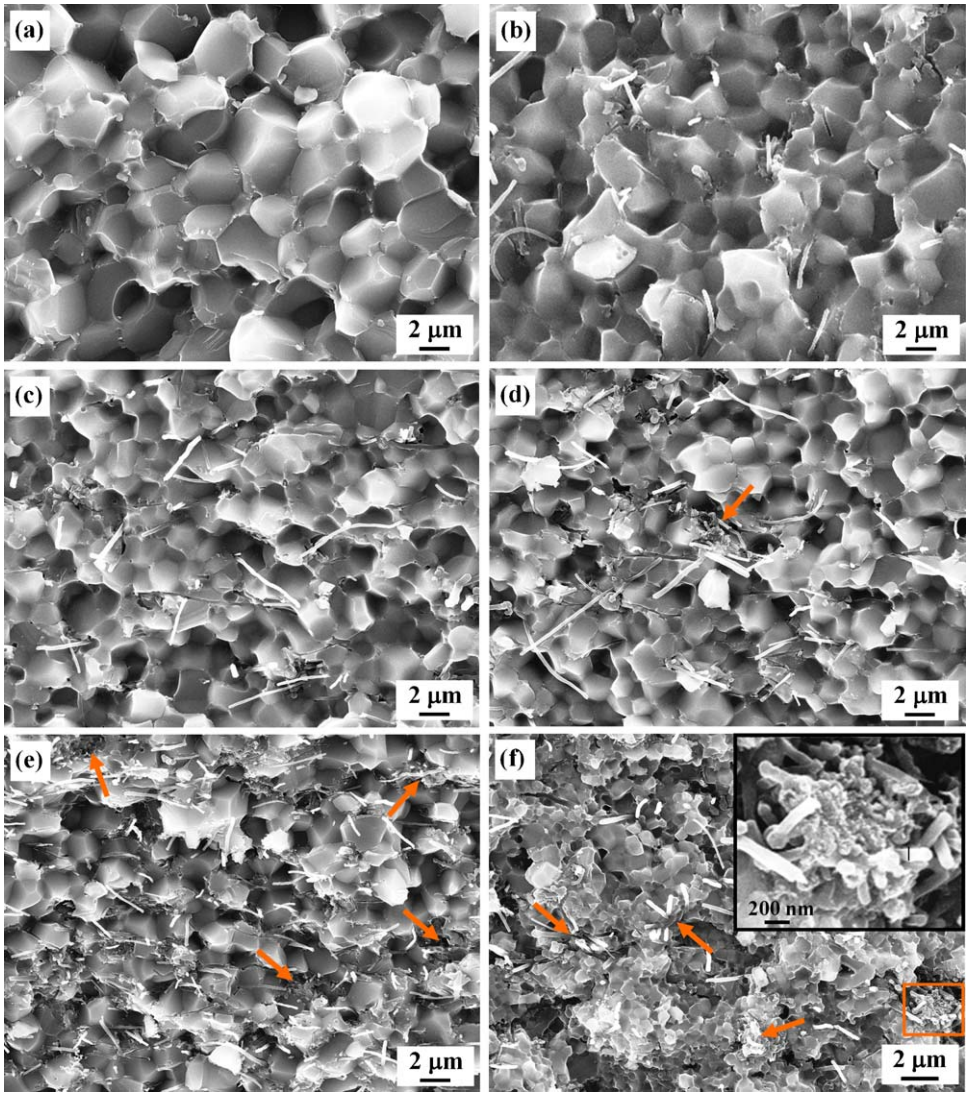

Fig. 4. SEM micrographs of fracture surfaces of CNFs/AlN composites: (a) monolithic AlN, (b) 1 wt.% CNFs/AlN, (c) 2 wt.% CNFs/AlN, (d) 3 wt.% CNFs/AlN, (e) 5 wt.% CNFs/AlN, (f) 7 wt.% CNFs/AlN (insert is a typical image of big CNFs clusters). (*Note:* The clusters are marked by arrows.)

CNFs during the crack propagation, which in turn resulted in the increase of fracture toughness. However, with the CNFs content further increased to 7 wt.%, the fracture toughness decreased to 3.76 MPa $m^{1/2}$. The decrease of fracture toughness might be ascribed to the poor interfacial bonding between the CNFs clusters and AlN matrix, which weakened the crack bridging effect of the CNFs considerably.

The flexural strength of the composites shows a trend similar to that of the fracture toughness, as demonstrated in Fig. 5(b). Addition of 2 wt.% CNFs improved the flexural strength of AlN-based ceramic by 13.4% from 312 MPa (without CNFs) to 354 MPa, which indicated the good strengthening effect of the CNFs. Concerning about flexure strength of inorganic polycrystalline materials, there is a linear relationship between strength (σ_f) and the inverse square root of grain size ($d^{-1/2}$), as expressed by the Hall–Petch equation:[23,24]

$$\sigma_f = \sigma_o + kd^{-1/2} \quad (1)$$

where σ_o and k are material constants. The smaller d is, the higher σ_f will be, if the densities of materials are not changed. Therefore, the former increment of σ_f might be due to the decrease in d of AlN grains with the almost same density (Table 1), and the latter reduction could be explained by the poor cohesion force between CNFs and AlN as well as the CNFs clusters existing in the composites.[25,26]

The hardness of CNFs/AlN composites decreased as the CNFs content increased (Fig. 5(c)). Many studies reported that the hardness could be improved in CNTs/ceramic system,[16–18,27] and the enhancement of the hardness was attributed to a strong bonding of CNTs and ceramic matrix grains, which could enable an effective load transfer from the matrix to the CNTs. However, on the fracture surfaces of the CNFs/AlN composites in the present case, some CNFs had been pulled-out, which reflected a certain degree of weakness of interfacial bonding between the CNFs and AlN matrix. In addition, the CNFs clusters existing in the intergranular of the compos-

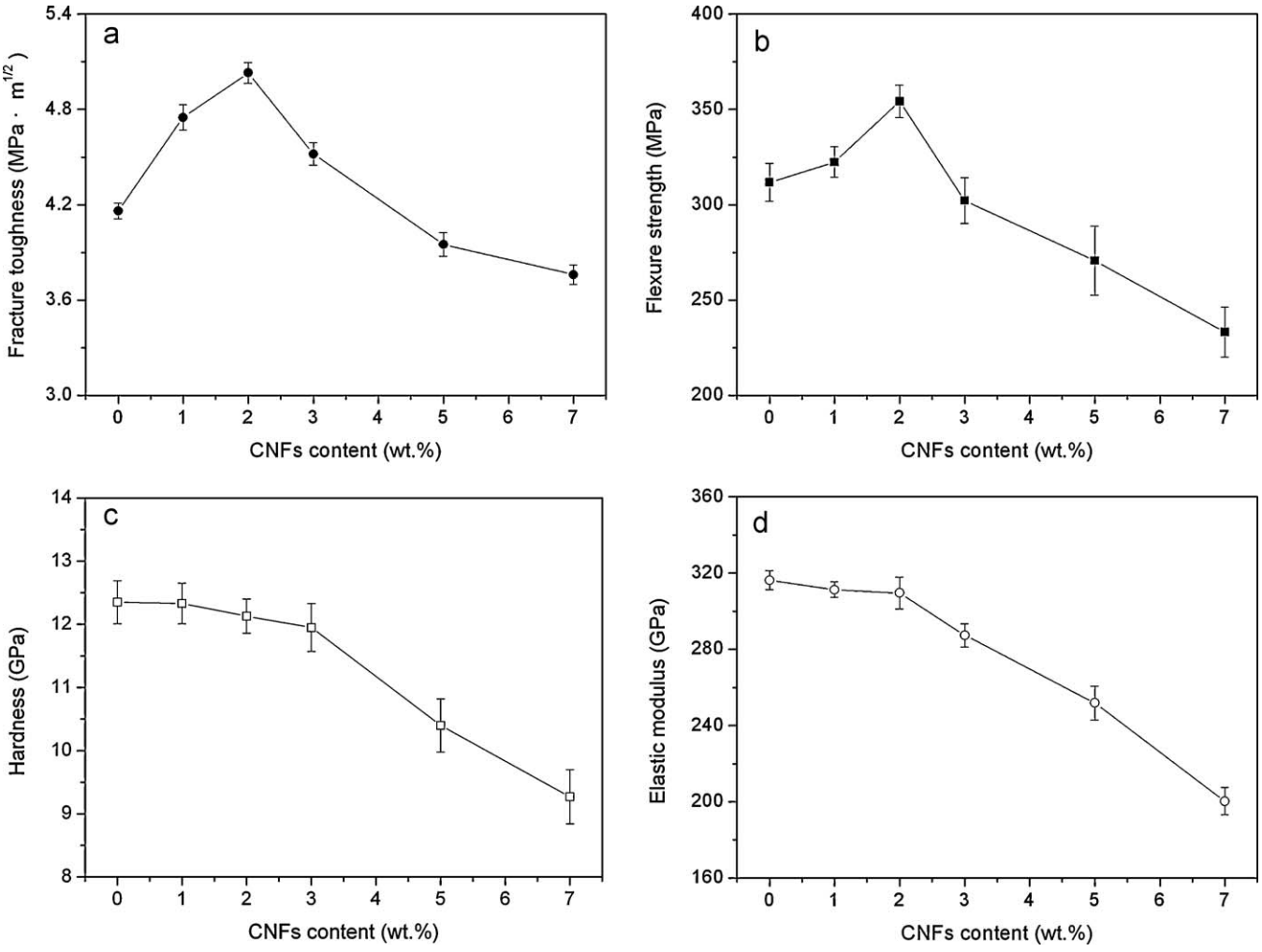

Fig. 5. Mechanical properties of CNFs/AlN composites: (a) fracture toughness, (b) flexural strength, (c) Vickers hardness and (d) elastic modulus.

ites that contained CNFs more than 3 wt.% would decrease the bonding strength of the AlN matrix (see Fig. 4(d)–(f)). Therefore, the addition of CNFs resulted in a lower hardness in the composites than in monolithic AlN (Fig. 5(c)). The elastic modulus of the composites followed the same trend as the hardness (Fig. 5(d)), presumably for the same reasons.

3.3. Electrical properties

Fig. 7 displays the DC electrical conductivity of the composites versus CNFs mass fraction, which suggests an increase of the conductivity along with the amount of CNFs in the composites. The conductivity was about 1.0×10^{-12} S m^{-1} for monolithic AlN, and it increased sharply when around 1 wt.% CNFs were

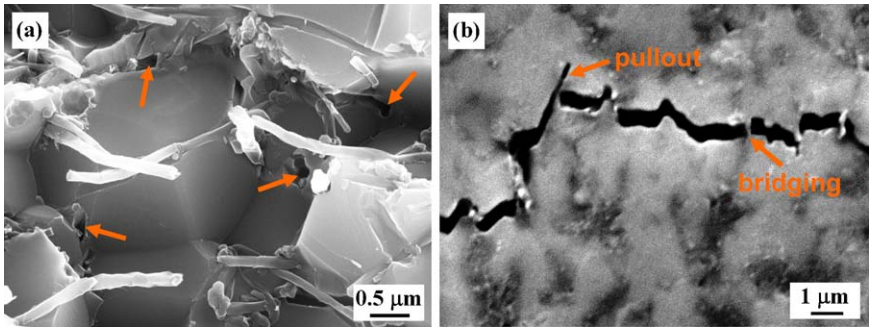

Fig. 6. SEM micrographs of 2 wt.% CNFs/AlN showing fracture surface after three point bending tests (a) and details of indentation crack propagation with CNFs pullout and bridging (b). (*Note:* The residual holes left by the pulling out of CNFs in Fig. 6(a) and CNFs pullout and bridging in Fig. 6(b) are marked by arrows.)

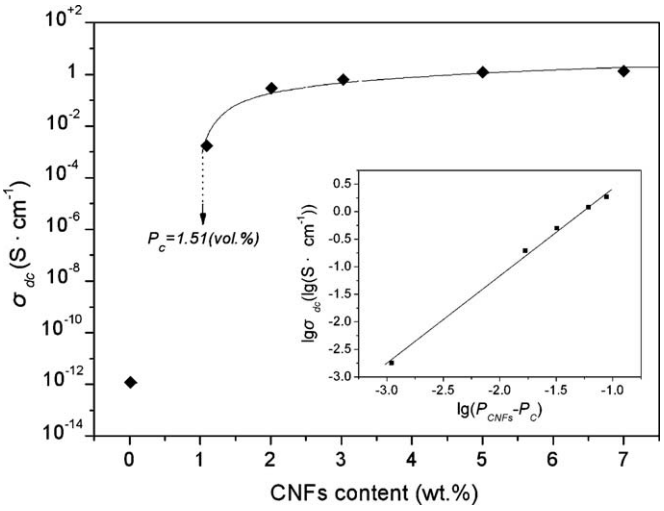

Fig. 7. DC Electrical conductivity σ_{dc} of CNFs/AlN composites as a function of CNFs content (insert: lgσ_{dc} plotted against lg($P_{\mathrm{CNFs}} - P_c$), where P_c is percolation threshold).

added. When the content of the CNFs increased to 2 wt.%, the conductivity increased to $\sim$0.2 S m^{-1}, and then it increased slightly with the further increase of CNFs content. The curve indicates a typical percolation behavior of the DC conductivity of the composites. According to the percolation theory,[28–30] when the conducting loading is above the percolation threshold, the DC conductivity of certain composites follows the scaling law as described by:

$$\sigma_{dc} = \sigma_c(P_{\mathrm{CNFs}} - P_c)^t, \quad \text{for } P_{\mathrm{CNFs}} > P_c, \tag{2}$$

where σ_{dc} and σ_c are the DC conductivities of the composites and the conducting component, respectively. P_{CNFs} is the volume fraction of the CNFs, P_c is the critical volume fraction or percolation threshold, and the exponent t reflects the dimensionality of the system. The t values of 1.30 and 1.94 are widely considered as corresponding to two and three dimensions, respectively.[31] In our study, by fitting the σ_{dc} values to Eq. (2), the percolation threshold P_c and exponent t were determined to be 1.51 ± 0.05 vol.% (about 0.93 wt.%) and 1.60 ± 0.06, respectively (see the insert of Fig. 7). The percolation threshold value calculated confirms our experimental results, and is similar to the value ($P_c \approx 1.50$ vol.%) of the CNFs/Al_2O_3 composites reported by Hiroaki et al.[5] and much higher than that of CNT/ceramic composites reported by Rul et al.[32] ($P_c \approx 0.64$ vol.% in SWCNT/$MgAl_2O_4$ composites) and Ahmad et al.[19] ($P_c \approx 0.79$ vol.% in MWCNT/Al_2O_3 composites). The difference is considered to be caused by the higher aspect ratio of CNTs compared with CNFs due to the inversely proportional relationship between the percolation threshold and the aspect ratio of conductive phase.[33] However, the t values normally lower than 1.94 would not be the sign of a two dimensional network but rather a result of thermally induced hopping transport between weakly connected parts of the network.[34]

4. Conclusions

In this study, carbon nanofibers/aluminum nitride (CNFs/AlN) composites were successfully prepared by plasma activated sintering (PAS). The experimental results reveal that CNFs have an important effect on the microstructure, mechanical and electrical properties of the composites. The SEM images show that the AlN grain growth is significantly inhibited by the CNFs. The flexural strength and fracture toughness of the composite containing 2 wt.% CNFs are obviously increased compared with those of monolithic AlN. The improvement of the fracture toughness can be attributed to the crack bridging and pullout, while the flexural strength improvement should be caused by the fine AlN grain size from the restrictive effect of the CNFs during PAS. Furthermore, the DC conductivity of the composites shows a typical percolation behavior with a very low percolation threshold at the CNFs content of about 0.93 wt.% (1.51 vol.%), suggesting that the CNFs sharply promote the electrical conductivity of the composites. Hence, CNFs are considered to be able to form a new generation of engineered CNFs/AlN composites with significantly improved mechanical and electrical properties.

Acknowledgements

This work was supported by the National Natural Science Foundation of China (No. 51002115), Research Fund for the Doctoral Program of Higher Education of China (No. 20100201120043) and Research Program for New Teacher of Xi'an Jiaotong University. The authors deeply appreciate the help of Ms. Qi Chen for the language promotion of the paper.

References

1. Mussler BH. Advanced materials and powders – aluminum nitride (AlN). *Am Ceram Soc Bull* 2000;**79**:45–7.
2. Sheppard LM. Aluminum nitride: a versatile but challenging material. *Am Ceram Soc Bull* 1990;**69**:1801–12.
3. Curtin WA, Sheldon BW. CNT-reinforced ceramics and metals. *Mater Today* 2004;**7**(11):44–9.
4. Kusunose T, Sekino T, Niihara K. Production of a grain boundary phase as conducting pathway in insulating AlN ceramics. *Acta Mater* 2007;**55**(18):6170–5.
5. Hiroaki S, Yuji K, Masaaki M, Chikashi I, Tetsuya K. Effects of adding Y_2O_3 on the electrical resistivity of aluminum nitride ceramics. *J Ceram Soc Jpn* 2008;**116**(4):566–71.
6. Ijima S. Helical microtubules of graphitic carbon. *Nature* 1991;**354**:56–8.
7. Merkoci A. Carbon nanotubes in analytical sciences. *Microchim Acta* 2006;**152**:157–74.
8. Melechko AV, Merkulov VI, McKnight TE, Guillorn MA, Klein KL, Lowndes DH, Simpson ML. Vertically aligned carbon nanofibers and related structures: controlled synthesis and directed assembly. *J Appl Phys* 2005;**97**:041301.
9. Maensiri S, Laokul P, Klinkaewnarong J, Amornkitbamrung V. Carbon nanofiber-reinforced alumina nanocomposites: fabrication and mechanical properties. *Mater Sci Eng A* 2007;**447**(1–2):44–50.
10. Hirota K, Hara H, Kato M. Mechanical properties of simultaneously synthesized and consolidated carbon nanofiber (CNF)-dispersed SiC composites by pulsed electric-current pressure sintering. *Mater Sci Eng A* 2007;**458**(1–2):216–25.

11. Kobayashi S, Kawai W. Development of carbon nanofiber reinforced hydroxyapatite with enhanced mechanical properties. *Compos Part A: Appl Sci Manuf* 2007;**38**(1):114–23.
12. Laurent C, Peigney A, Dumortier O, Rousset A. Carbon nanotubes–Fe–Alumina nanocomposites. Part II. Microstructure and mechanical properties of the hot-Pressed composites. *J Eur Ceram Soc* 1998;**18**(14):2005–13.
13. Zhan GD, Mukherjee AK. Carbon nanotube reinforced alumina-based ceramics with novel mechanical, electrical, and thermal properties. *Int J Appl Ceram Technol* 2004;**1**(2):161–71.
14. Zhan GD, Kuntz JD, Garay JE, Mukherjee AK, Zhu P, Koumoto K. Thermoelectric properties of carbon nanotube/ceramic nanocomposites. *Scripta Mater* 2006;**54**(1):77–82.
15. Wang XT, Padture NP, Tanaka H. Contact-damage-resistant ceramic/single-wall carbon nanotubes and ceramic/graphite composites. *Nat Mater* 2004;**3**:539–44.
16. Cha SI, Kim KT, Lee KH, Mo CB, Hong SH. Strengthening and toughening of carbon nanotube reinforced alumina composite fabricated by molecular level mixing process. *Scripta Mater* 2005;**53**(7):793–7.
17. Zhang T, Kumari L, Du GH, Li WZ, Wang QW, Balani K, Agarwal A. Mechanical properties of carbon nanotube–alumina composites synthesized by chemical vapor deposition and spark plasma sintering. *Compos Part A: Appl Sci Manuf* 2009;**40**(1):86–93.
18. Peigney A, Garcia FL, Estourne's C, Weibel A, Laurent C. Toughening and hardening in double-walled carbon nanotube/nanostructured magnesia composites. *Carbon* 2010;**48**(7):1952–60.
19. Ahmad K, Pan W, Shi SL. Electrical conductivity and dielectric properties of multiwalled carbon nanotube and alumina composites. *Appl Phys Lett* 2006;**89**(13):133122.
20. Balázsi C, Shen Z, Kónya Z, Kasztovszky Z, Wéber F, Vértesy Z, Biró LP, Kiricsi I, Arató P. Processing of carbon nanotube reinforced silicon nitride composites by spark plasma sintering. *Compos Sci Technol* 2005;**65**(5):727–33.
21. Dusza J, Blugan G, Morgiel J, Kuebler J, Inam F, Peijs T, Reece MJ, Puchy V. Hot pressed and spark plasma sintered zirconia/carbon nanofiber composites. *J Eur Ceram Soc* 2009;**29**(15):3177–84.
22. Qiao L, Zhou H, Xue H, Wang S. Effect of Y_2O_3 on low temperature sintering and thermal conductivity of AlN ceramics. *J Eur Ceram Soc* 2003;**23**(1):61–7.
23. Hall EO. The deformation and ageing of mild steel: III discussion of results. *Proc Phys Soc B* 1951;**64**(9):747–53.
24. Petch NJ. The cleavage strength of polycrystals. *J Iron Steel Inst* 1953;**174**:25–8.
25. Hirota K, Takaura Y, Kato M, Miyamoto Y. Fabrication of carbon nanofiber (CNF)-dispersed Al_2O_3 composites by pulsed electric-current pressure sintering and their mechanical and electrical properties. *J Mater Sci* 2007;**42**:4792–800.
26. Shimoda K, Hinoki T, Kohyama A. Effect of carbon nanofibers (CNFs) content on thermal and mechanical properties of CNFs/SiC nanocomposites. *Compos Sci Technol* 2010;**70**(2):387–92.
27. Mo CB, Cha SI, Kim KT, Lee KH, Hong SH. Fabrication of carbon nanotube reinforced alumina matrix nanocomposite by sol–gel process. *Mater Sci Eng A* 2005;**395**(1-2):124–8.
28. Bergman DJ. Exactly solvable microscopic geometries and rigorous bounds for the complex dielectric constant of a two-component composite material. *Phys Rev Lett* 1980;**44**:1285–7.
29. Nan CW. Physics of inorganic inhomogeneous materials. *Prog Mater Sci* 1993;**37**:1–116.
30. Meir Y. Percolation-type description of the metal–insulator transition in two dimensions. *Phys Rev Lett* 1999;**83**:3506–9.
31. Stauffer D. *Introduction to the Percolation Theory*. London and Philadelphia: Taylor & Francis; 1985.
32. Rul S, Lefevre-schlick F, Capria E, Laurent C, Peigney A. Percolation of single-walled carbon nanotubes in ceramic matrix nanocomposites. *Acta Mater* 2004;**52**(4):1061–7.
33. Flahaut E, Peigney A, Laurent C, Marliere C, Chastel F, Rousset A. Carbon nanotube–metal–oxide nanocomposites: microstructure, electrical conductivity and mechanical properties. *Acta Mater* 2000;**48**(14):3803–12.
34. Kilbride BE, Coleman JN, Fraysse F, Fournet P, Cadek M, Drury A, Hutzler S, Roth S, Blau WJ. Experimental observation of scaling laws for alternating current and direct current conductivity in polymer–carbon nanotube composite thin films. *J Appl Phys* 2002;**92**:4024.